Dispersive transport and symmetry of the dispersion tensor in porous media

Steven R. Pride[*] and Donald W. Vasco[†]
Lawrence Berkeley National Laboratory, Energy Geosciences Division, 1 Cyclotron Road, MS 74R316C, Berkeley, California 94720, USA

Eirik G. Flekkoy[‡]
Department of Physics, University of Oslo, P.O. Box 1043 Blindern, 0316 Oslo, Norway

Ran Holtzman[§]
Robert H. Smith Faculty of Agriculture, Food and Environment, Hebrew University of Jerusalem, P.O. Box 12, Rehovot 76100, Israel
(Received 29 November 2016; published 10 April 2017)

The macroscopic laws controlling the advection and diffusion of solute at the scale of the porous continuum are derived in a general manner that does not place limitations on the geometry and time evolution of the pore space. Special focus is given to the definition and symmetry of the dispersion tensor that is controlling how a solute plume spreads out. We show that the dispersion tensor is not symmetric and that the asymmetry derives from the advective derivative in the pore-scale advection-diffusion equation. When flow is spatially variable across a voxel, such as in the presence of a permeability gradient, the amount of asymmetry can be large. As first shown by Auriault [J.-L. Auriault *et al.*, Transp. Porous Med. **85**, 771 (2010)] in the limit of low Péclet number, we show that at any Péclet number, the dispersion tensor D_{ij} satisfies the flow-reversal symmetry $D_{ij}(+\mathbf{q}) = D_{ji}(-\mathbf{q})$ where $\mathbf{q}$ is the mean flow in the voxel under analysis; however, Reynold's number must be sufficiently small that the flow is reversible when the force driving the flow changes sign. We also demonstrate these symmetries using lattice-Boltzmann simulations and discuss some subtle aspects of how to measure the dispersion tensor numerically. In particular, the numerical experiments demonstrate that the off-diagonal components of the dispersion tensor are antisymmetric which is consistent with the analytical dependence on the average flow gradients that we propose for these off-diagonal components.

DOI: 10.1103/PhysRevE.95.043103

I. INTRODUCTION

In a porous material, if fluid injection at some point creates a localized change in solute concentration (or indeed any fluid property) and if there is flow taking place either due to the injection process alone or an already existent background flow (or both), this change in solute concentration will be transported downstream by the flow, spreading out into a plume in the process. The flux due to the solute being carried along by the average flow in each voxel of porous material is called advection while the flux that results in the spreading out into a plume is called dispersion.

This article is concerned with establishing the mass conservation and transport laws that describe such dispersive transport at the scale of the porous continuum. Such laws are important in the modeling of how contaminants and tracers spread out in the Earth's subsurface [1–4] and in a diverse range of medical and industrial applications from modeling how drugs and other solutes move through biological tissue [5] to modeling filtration processes across porous membranes [6]. Thousands of articles over the past 50-plus years have used seemingly reasonable forms of the porous-continuum solute transport laws; comprehensive overviews have been provided by Bear [1], de Marsily [2], Dullien [3], and Sahimi [4] among others. Due to differences in the proposed transport laws when fluid density and porosity are allowed to vary in time, we provide in this paper a systematic derivation of the porous-continuum dispersive transport equations. We place particular emphasis on the definition and symmetry properties of the dispersion tensor. An important aspect of this work is the consideration of the nature of the off-diagonal terms of the dispersion tensor that are generally ignored when one of the coordinate directions aligns with the flow direction and the material is isotropic. Our analytical considerations are verified using lattice-Boltzmann simulations of the transport process.

To understand the physical essence of what dispersion and the dispersion tensor is representing, consider a small plume of excess solute in a porous material. Steady flow in the porous material is being driven by a directed force. Where the concentration gradient of the plume is perpendicular to the mean flow direction, as the local flow bifurcates around a grain, fluid with a given concentration is both advected into a pore up the concentration gradient and into a pore down the concentration gradient. The up-gradient pore has its concentration lowered by this process and the down-gradient pore has its concentration increased which corresponds to solute flux down the concentration gradient. This is called transverse mechanical dispersion. Where the concentration gradient of the plume is parallel with the mean flow direction, the local flow in the center of the pores is greater than near the solid grain boundaries which results in advection enhanced solute diffusion that is analogous to Taylor-Aris dispersion [7] in a tube and is called longitudinal mechanical dispersion. Recent numerical simulations [8,9] of the pore-scale longitudinal and transverse mechanical dispersion through

[*]srpride@lbl.gov
[†]dwvasco@lbl.gov
[‡]e.g.flekkoy@fys.uio.no
[§]holtzman.ran@mail.huji.ac.il

numerical reconstructions of actual sedimentary porous media give greater insight into the dependence on the pore geometry.

In addition to the above two sources of dispersion, there is also the usual random-walk diffusion that transports solute down the concentration gradient. In a porous continuum, the effects of mechanical dispersion and diffusion are combined into a single dispersion tensor. Comparing a characteristic advection with flow speed U to a characteristic diffusion with diffusivity D_m taking place over a length scale ℓ (typical grain size) defines the Péclet number $\mathrm{Pe} = U\ell/D_m$. When $\mathrm{Pe} \gg 1$, mechanical dispersion dominates diffusion.

There can also be mechanical dispersion in a direction perpendicular to the concentration gradient even in an isotropic material. This effect has generally not received as much attention in the literature and is responsible for the presence of off-diagonal terms in the dispersion tensor even when one of the coordinate directions is parallel with the macroscopic flow direction. We show that these off-diagonal terms are not symmetric when present. This paper will place an emphasis on considering this "nonstandard" type of mechanical dispersion, propose what it is most commonly due to (gradients in flow across a voxel) and derive a flow-reversal symmetry that these off-diagonal terms must obey. Such off-diagonal terms are a complicated coupling between advection and diffusion and increase from zero with increasing Péclet number.

The macroscopic (porous continuum) governing equations for nonreactive solute transport have been obtained and presented in different ways [10–14]; however, there are some differences between presentations on how to define the concentration of solute and where factors of porosity and fluid density arrive in the equations if porosity and fluid density are allowed to vary in time and space. Porosity changes in time are caused by deformation of the framework of grains associated with the fluid injection. For two-space homogenization methods [13,14], there is required to be an explicit separation of scales into pore dimensions ℓ and macroscopic dimensions L so that a small parameter $\epsilon = \ell/L$ exists that can be used to truncate an asymptotic development of the pore-scale fields. We are interested in an approach that is valid when there are more than two length scales present so that two-space homogenization is not formally applicable. Further, the boundary conditions on the individual voxels tend to be periodic in homogenization approaches while Dirichlet conditions on the solute concentration are the natural ones to connect to.

II. MACROSCOPIC RESPONSE OF A VOXEL

We begin with some general considerations of the average (macroscopic) response in porous media.

Figure 1 depicts a voxel of porous material $\Omega(\mathbf{r})$ located at position $\mathbf{r} = r_1\hat{\mathbf{x}}_1 + r_2\hat{\mathbf{x}}_2 + r_3\hat{\mathbf{x}}_3$ within a larger porous system. For fields distributed at points $\mathbf{x} = x_1\hat{\mathbf{x}}_1 + x_2\hat{\mathbf{x}}_2 + x_3\hat{\mathbf{x}}_3$ throughout the interior of the voxel, the macroscopic description requires only the average of these fields and the gradient of the average across the voxel. We can consider an averaging voxel of any shape but there is no loss in generality in considering a simple cube of volume L^3. The six bounding faces of the voxel $\partial\Omega$ are located at $x_i = \pm L/2$ for $i = 1,2,3$. The pore space within Ω is denoted Ω_p and the intersection

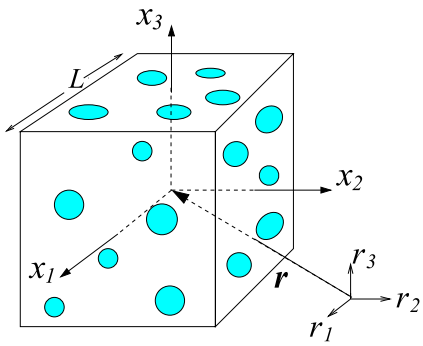

FIG. 1. A cubic voxel of porous material $\Omega(\mathbf{r})$ centered on point $\mathbf{r} = (r_1,r_2,r_3)$ within the larger porous system and having local coordinates $\mathbf{x} = (x_1,x_2,x_3)$ as shown.

of the pore space with the external surface of the voxel is denoted $\partial\Omega_{pe}$.

Consider first a scalar field $\psi(\mathbf{x})$ associated with the pore space (density, pressure, temperature, etc.). The average of this field throughout the pore space is

$$\overline{\psi}(\mathbf{r}) = \frac{1}{V_p(\mathbf{r})}\int_{\Omega_{pe}(\mathbf{r})} \psi(\mathbf{x})\, d^3\mathbf{x}, \tag{1}$$

where V_p is the pore volume. The porosity is defined

$$\phi(\mathbf{r}) = \frac{V_p(\mathbf{r})}{L^3} \tag{2}$$

and may possess a macroscopic gradient. We generally expect that an average field $\overline{\psi}$ at a point $\mathbf{r}$ will change as the size L of the averaging voxel changes.

In addition to the volume average $\overline{\psi}$, there is assumed to be present a macroscopic gradient $\nabla\overline{\psi}$ across the voxel where $\nabla = \partial/\partial\mathbf{r}$ is the gradient operator acting on volume-averaged quantities. The gradient of a quantity averaged throughout a voxel is the difference in the volume integrals for voxels centered at $\mathbf{r}$ and $\mathbf{r} + d\mathbf{r}$. In the limit as $d\mathbf{r} \to 0$, the difference in the two volume integrals becomes an integral over the bounding surface involving the outward normal $\mathbf{n}$ to the surface. The exact theorem is (e.g., Ref. [12] or [15])

$$\nabla[\phi\overline{\psi}] = \frac{1}{L^3}\int_{\partial\Omega_{pe}} \mathbf{n}\,\psi(\mathbf{x})\, d^2\mathbf{x}. \tag{3}$$

Upon inserting $\psi = 1$, we obtain the definition of the macroscopic porosity gradient

$$\nabla\phi = \frac{1}{L^3}\int_{\partial\Omega_{pe}} \mathbf{n}\, d^2\mathbf{x}. \tag{4}$$

Equation (3) can then be rewritten to give directly the gradient of a field averaged over the pore space

$$\nabla\overline{\psi}(\mathbf{r}) = \frac{1}{\phi(\mathbf{r})L^3}\int_{\partial\Omega_{pe}} \mathbf{n}\,[\psi(\mathbf{x}) - \overline{\psi}(\mathbf{r})]\, d^2\mathbf{x}. \tag{5}$$

Simply and intuitively, when the field being averaged is larger on one side of an averaging region compared to the opposing side, there is a macroscopic gradient present.

Consider next a vector flux $\mathbf{j}(\mathbf{x})$ taking place through the pore space (fluid flow, solute flux, etc.). The average flux

through the pore space is

$$\bar{\mathbf{j}}(\mathbf{r}) = \frac{1}{\phi(\mathbf{r})L^3}\int_{\Omega_p} \mathbf{j}(\mathbf{x})\, d^3\mathbf{x} \tag{6}$$

so that the theorem of Eq. (3) yields the macroscopic divergence theorem for pore-averaged fields

$$\nabla\cdot[\phi\,\bar{\mathbf{j}}] = \frac{1}{L^3}\int_{\partial\Omega_{pe}} \mathbf{n}\cdot\mathbf{j}(\mathbf{x})\, d^2\mathbf{x}. \tag{7}$$

Again using Eq. (4) for the porosity gradient, we rewrite Eq. (7) as

$$\nabla\cdot\bar{\mathbf{j}}(\mathbf{r}) = \frac{1}{\phi(\mathbf{r})L^3}\int_{\partial\Omega_{pe}} \mathbf{n}\cdot[\mathbf{j}(\mathbf{x}) - \bar{\mathbf{j}}(\mathbf{r})]\, d^2\mathbf{x}. \tag{8}$$

So either the macroscopic divergence of an average vector flux or the macroscopic gradient of an average scalar field are independent of the average value of the field throughout the pore space.

III. CONSERVATION OF FLUID MASS

We now use the above formalism to derive the macroscopic statement of the conservation of fluid mass. The pertinent local fields throughout the pore space are $\rho(\mathbf{x})$ the local solution mass density and $\mathbf{u}(\mathbf{x})$ the local solution flow velocity. The conservation of solution mass for the voxel can be written

$$-\frac{\partial}{\partial t}\left[\int_{\Omega_p}\rho\, d^3\mathbf{x}\right] = \int_{\partial\Omega_{pe}}\mathbf{n}\cdot\mathbf{u}\,\rho\, d^2\mathbf{x}. \tag{9}$$

After dividing both sides by L^3, the left-hand side is identified as

$$\frac{\partial}{\partial t}\left[\frac{V_p}{L^3}\frac{1}{V_p}\int_{\Omega_p}\rho\, d^3\mathbf{x}\right] = \frac{\partial}{\partial t}[\phi\overline{\rho}]. \tag{10}$$

When treating the integral of the right-hand side, we use the divergence theorem of Eq. (7) along with the decompositions throughout Ω_p

$$\mathbf{u} = \overline{\mathbf{u}} + \delta\mathbf{u}(\mathbf{x}), \tag{11}$$

$$\rho = \overline{\rho} + \delta\rho(\mathbf{x}) \tag{12}$$

to obtain

$$-\frac{\partial}{\partial t}[\phi\overline{\rho}] = \nabla\cdot\left[\frac{1}{L^3}\int_{\Omega_p}(\overline{\rho}+\delta\rho)(\overline{\mathbf{u}}+\delta\mathbf{u})\, d^3\mathbf{x}\right] \tag{13}$$

$$= \nabla\cdot[\phi\,\overline{\rho}\,\overline{\mathbf{u}}] + \nabla\cdot\left[\frac{1}{L^3}\int_{\Omega_p}\delta\rho\,\delta\mathbf{u}\, d^3\mathbf{x}\right]. \tag{14}$$

We have used that $\int_{\Omega_p}\delta\mathbf{u}\, d^3\mathbf{x} = 0$ and $\int_{\Omega_p}\delta\rho\, d^3\mathbf{x} = 0$.

The second term on the right-hand side of Eq. (14) is nonstandard; i.e., it is usually not a part of the macroscopic statement of fluid-mass conservation at the porous-continuum level. It represents a dispersive flux of fluid mass that is distinct from the average mass flux $\phi\,\overline{\rho}\,\overline{\mathbf{u}}$ that is allowed for in the first term on the right-hand side. The way that deviations in solution density $\delta\rho$ develop is if there are deviations in fluid pressure and solute concentration. There is a state function $\rho = \rho(p,\varphi)$ for every (isothermal) solution, where p is the local fluid pressure and φ the local solute concentration (as defined in the next section).

When there is a strong macroscopic pressure gradient $\nabla\overline{p}$ and/or concentration gradient ∇c present (the macroscopic concentration measure c is defined in the next section), one can imagine that there is a strong enough macroscopic gradient in solution density $\nabla\overline{\rho}$ to warrant allowing for the deviations $\delta\rho(\mathbf{x})$ at the local level and the macroscopic dispersive total-mass-flux vector $\mathbf{J}_\rho$ defined by

$$\mathbf{J}_\rho = \frac{1}{L^3}\int_{\Omega_p}\delta\rho\,\delta\mathbf{u}\, d^3\mathbf{x} \tag{15}$$

$$= -\mathbf{D}_\rho\cdot\nabla\overline{\rho} \tag{16}$$

$$= -\mathbf{D}_\rho\cdot\left(\frac{\partial\overline{\rho}}{\partial\overline{p}}\nabla\overline{p} + \frac{\partial\overline{\rho}}{\partial c}\nabla c\right). \tag{17}$$

The solution-mass dispersion tensor $\mathbf{D}_\rho$ (units of diffusivity) is defined through the above equations. Its components will be nonzero to the extent that flow-velocity gradients are present across a voxel (that generate $\delta\mathbf{u}$) and to the extent that solution density gradients are present across a voxel (that generate $\delta\rho$) so that the product $\delta\rho\,\delta\mathbf{u}$ does not simply average to zero throughout the pore space.

For an average flow in the x direction created by a macroscopic pressure gradient in the x direction that in turn has a gradient in the y direction, we can make the order-of-magnitude estimate that

$$|\mathbf{J}_\rho| = \frac{k}{\eta}\left|\frac{\partial^2\overline{p}}{\partial x\,\partial y}\right| L\left(\frac{\partial\overline{\rho}}{\partial\overline{p}}|\Delta\overline{p}| + \frac{\partial\overline{\rho}}{\partial c}|\Delta c|\right), \tag{18}$$

where L is the size of a voxel of porous material, k is the Darcy permeability and η is the solution viscosity. We can further estimate the advective flux as

$$|\mathbf{J}_a| = \frac{k}{\eta}\left|\frac{\partial\overline{p}}{\partial x}\right|\overline{\rho}. \tag{19}$$

With the estimate $|\partial(\partial\overline{p}/\partial x)\partial y| \approx |\partial\overline{p}/\partial x|/L$, the importance of dispersive solution-mass flux compared to the advective flux is given by the order-of-magnitude dimensionless ratio

$$\frac{|\mathbf{J}_\rho|}{|\mathbf{J}_a|} = \frac{|\Delta\overline{p}|}{\overline{\rho}\,c_p^2} + \frac{(\partial\overline{\rho}/\partial c)|\Delta c|}{\overline{\rho}}, \tag{20}$$

where we used that the speed of sound c_p in the solution is $c_p^2 = \overline{\rho}\,\partial\overline{p}/\partial\overline{\rho}$. Because $\overline{\rho}\,c_p^2 \approx 10^9$ Pa for liquids, so long as the pressure deviations across a voxel are much smaller than 10^9 Pa, which they will be in all applications of flow in porous media, we can ignore the solution-mass dispersion due to pressure gradients. The relation between the solute-mass to solution-mass ratio c and the molarity M (mol/l) of the solution is $M = \overline{\rho}c/\mu$ where μ is the molecular weight of the solute as read from the periodic table in grams per mole. We thus have to leading order-of-magnitude that $\Delta c \approx 10^{-2}(\text{l/mol})\Delta M$. For saline solutions at ambient pressure and temperature, the appendix of Ref. [16] shows that $\partial\overline{\rho}/\partial c \approx 10^3$ kg/m$^3 \approx \overline{\rho}$. Further, a very large molarity change across a porous voxel would be on the order of $\Delta M \approx 10^{-1}$ mol/l, so that perhaps the largest value we can expect for the ratio $|\mathbf{J}_\rho|/|\mathbf{J}_a|$ is on the order 10^{-3} which we will assume is negligible.

We thus feel justified in writing the conservation of mass in a porous continuum in the standard form

$$-\frac{\partial}{\partial t}[\phi\overline{\rho}] = \nabla\cdot[\phi\,\overline{\rho}\,\overline{\mathbf{u}}] - \overline{\rho}_s Q_s \delta(\mathbf{r}-\mathbf{r}_s), \tag{21}$$

where a source term has been included to represent solution of density $\overline{\rho}_s$ being injected into the porous material at the voxel positioned at $\mathbf{r}_s$ and at a volumetric rate Q_s (m^3/s). If solution is being withdrawn ($Q_s < 0$), then the density to use at the withdrawal voxel is simply the $\overline{\rho}$ locally present.

Instead of the average fluid velocity $\overline{\mathbf{u}}$, we are usually modeling both the Darcy velocity $\mathbf{q}$ (flux through the porous material of fluid relative to the solid) and the average solid velocity $\overline{\mathbf{v}}_s$ at the macroscopic scale of the porous continuum (if poroelastic deformation is being allowed for). We have the definitions that

$$\mathbf{q} = \phi(\overline{\mathbf{u}} - \overline{\mathbf{v}}_s) \tag{22}$$

and

$$\overline{\mathbf{v}}_s = \frac{1}{V_s}\int_{\Omega_s}\mathbf{v}_s(\mathbf{x})\,d^3\mathbf{x}. \tag{23}$$

In terms of $\mathbf{q}$ and $\overline{\mathbf{v}}_s$, we can then distribute derivatives in Eq. (21) to obtain

$$\frac{\partial\phi}{\partial t} + \overline{\mathbf{v}}_s\cdot\nabla\phi + \frac{\phi}{\overline{\rho}}\left[\frac{\partial\overline{\rho}}{\partial t} + \left(\frac{\mathbf{q}}{\phi} + \overline{\mathbf{v}}_s\right)\cdot\nabla\overline{\rho}\right]$$
$$= -\nabla\cdot\mathbf{q} - \phi\nabla\cdot\overline{\mathbf{v}}_s - \frac{\overline{\rho}_s}{\overline{\rho}}Q_s\delta(\mathbf{r}-\mathbf{r}_s), \tag{24}$$

which may also be thought of as the differential equation that determines how porosity changes,

As such, we can also derive Eq. (24) in an alternative manner dropping the injection point source for convenience. Writing the porosity as $\phi = V_p/V$ (ratio of pore volume to total volume associated with a given mass element of porous material), we take a total derivative to obtain

$$\frac{d\phi}{dt} = \frac{1}{V}\frac{dV_p}{dt} - \frac{V_p}{V^2}\frac{dV}{dt} = \frac{1}{V}\frac{dV_p}{dt} - \frac{\phi}{V}\frac{dV}{dt}. \tag{25}$$

The change in the pore volume is exactly the difference between how much fluid enters or leaves an element and how much the fluid within the pores compresses or dilates. As was initially assumed by Biot and Willis [17] and later proven by Pride and Berryman [15], the rate that fluid volume is accumulating in a porous element divided by the volume of the element is given by $-\nabla\cdot\mathbf{q}$. The rate that the fluid volume is compressing (causing an increase in fluid density) divided by the sample volume is $(\phi/\overline{\rho})d\overline{\rho}/dt$. Reference [15] further demonstrates that $\nabla\cdot\overline{\mathbf{v}}_s = (dV/dt)/V$. We thus obtain

$$\frac{d\phi}{dt} + \frac{\phi}{\overline{\rho}}\frac{d\overline{\rho}}{dt} = -\nabla\cdot\mathbf{q} - \phi\nabla\cdot\mathbf{v}_s. \tag{26}$$

Comparing this expression to the earlier statement of Eq. (24), we can identify with confidence the nature of the total derivatives

$$\frac{d\phi}{dt} = \frac{\partial\phi}{\partial t} + \overline{\mathbf{v}}_s\cdot\nabla\phi, \tag{27}$$

$$\frac{d\overline{\rho}}{dt} = \frac{\partial\overline{\rho}}{\partial t} + \left(\frac{\mathbf{q}}{\phi} + \overline{\mathbf{v}}_s\right)\cdot\nabla\overline{\rho}. \tag{28}$$

In particular, these expressions unambiguously identify the velocity vectors to be used in the advective derivatives when both fluid and solid are allowed to move and deform. Quantities that are associated with the porous frame, like porosity and permeability, use the average solid velocity in the advective derivative and those that are associated with the fluid, like the average fluid density, use the average fluid velocity ($\overline{\mathbf{u}} = \mathbf{q}/\phi + \overline{\mathbf{v}}_s$).

IV. CONSERVATION OF SOLUTE MASS

We next derive the conservation of solute mass in a porous material. Keeping track of the solute entering and leaving the cubic voxel we have

$$-\frac{\partial}{\partial t}\left[\int_{\Omega_p}\rho\varphi\,d^3\mathbf{x}\right] = \int_{\partial\Omega_p}\mathbf{n}\cdot[-\rho D_m\nabla\varphi + \rho\varphi\mathbf{u}]\,d^2\mathbf{x}, \tag{29}$$

where φ is the concentration of solute expressed as a mass ratio (mass of solute divided by mass of solution) and D_m is the molecular diffusivity. The first flux term in brackets is diffusion and the second is advection. In assuming the diffusion to be described by Fick's law, we are implicitly assuming the mean-free-path length λ of the random movement of solute particles is much smaller than the pore sizes. Because λ is on the order of molecular dimensions for liquid solvents, Fick's law always provides an accurate description of the solute diffusion within the pores.

As the macroscopic measure of concentration, we introduce

$$c = \frac{\int_{\Omega_p}\rho\varphi\,d^3\mathbf{x}}{\int_{\Omega_p}\rho\,d^3\mathbf{x}} = \frac{\overline{\rho\varphi}}{\overline{\rho}}. \tag{30}$$

We further write the local concentration $\varphi(\mathbf{x})$ throughout the pore space as

$$\varphi(\mathbf{x}) = c + \delta\varphi(\mathbf{x}) \tag{31}$$

and continue to use $\mathbf{u}(\mathbf{x}) = \overline{\mathbf{u}} + \delta\mathbf{u}(\mathbf{x})$ for the flow field. Upon substituting Eq. (31) into the definition of c, we obtain that the deviations $\delta\varphi(\mathbf{x})$ satisfy

$$\int_{\Omega_p}\rho(\mathbf{x})\delta\varphi(\mathbf{x})\,d^3\mathbf{x} = 0 \tag{32}$$

or $\overline{\delta\varphi} = 0$ under conditions where $\rho(x) = \overline{\rho}$ is a uniform spatial constant within Ω_p.

The pore-scale boundary-value problem for $\varphi(\mathbf{x})$ is [18]

$$\frac{\partial\varphi}{\partial t} + \mathbf{u}\cdot\nabla\varphi = \frac{1}{\rho}\nabla\cdot(\rho D_m\nabla\varphi) \text{ in } \Omega_p \tag{33}$$

subject to the boundary conditions on the six bounding cube faces that

$$\varphi(\mathbf{x}) = c_o \pm \Delta c_i \quad \text{on } x_i = \pm\frac{L}{2} \tag{34}$$

and $\mathbf{n}\cdot\nabla\varphi = 0$ on the grain surfaces ∂G. The Δc_i are defined from the macroscopic concentration gradient as

$$\nabla c = \hat{\mathbf{x}}_1\frac{\Delta c_1}{L} + \hat{\mathbf{x}}_2\frac{\Delta c_2}{L} + \hat{\mathbf{x}}_3\frac{\Delta c_3}{L}. \tag{35}$$

When all the $\Delta c_i = 0$, we have that $\varphi(\mathbf{x}) = c_o$ is the solution of Eqs. (33) and (34) in which case $c = c_o$. When any of the $\Delta c_i \neq 0$ in the presence of advective flow, we can have $c \neq c_o$.

Upon dividing both sides of the solute mass balance of Eq. (29) by L^3 and introducing the above definitions, we have

$$-\frac{\partial}{\partial t}[\phi\overline{\rho}c] = \frac{1}{L^3}\int_{\partial\Omega_p} \mathbf{n}\cdot[-\rho D_m \nabla\delta\varphi + \rho(c+\delta\varphi)\mathbf{u}]\, d^2\mathbf{x}. \tag{36}$$

The term on the right-hand side that involves $\mathbf{n}\cdot\rho c\mathbf{u}$ becomes $\nabla\cdot(\phi\overline{\rho}c\overline{\mathbf{u}})$ according to the mass balance of Eqs. (9) and (21). The macroscopic divergence theorem of Eq. (7) then results in

$$-\frac{\partial}{\partial t}[\phi\overline{\rho}c] = \nabla\cdot(\phi\overline{\rho}c\overline{\mathbf{u}}) + \nabla\cdot\left[\frac{1}{L^3}\int_{\Omega_p}\rho[-D_m\nabla\delta\varphi + \delta\varphi(\overline{\mathbf{u}}+\delta\mathbf{u})]\, d^3\mathbf{x}\right]. \tag{37}$$

Because $\overline{\mathbf{u}}$ is a uniform constant throughout the pore space, the integral of $\rho\delta\varphi$ throughout the pore space is zero according to Eq. (32). A final application of the total mass balance of Eq. (21) then yields the macroscopic statement of conservation of solute

$$\frac{\partial c}{\partial t} + \overline{\mathbf{u}}\cdot\nabla c = -\frac{1}{\phi\overline{\rho}}\nabla\cdot\mathbf{J}, \tag{38}$$

where the dispersive solute-mass flux vector $\mathbf{J}$ is defined

$$\mathbf{J} = \frac{1}{L^3}\int_{\Omega_p}\rho[-D_m\nabla\delta\varphi + \delta\varphi\delta\mathbf{u}]\, d^3\mathbf{x}. \tag{39}$$

The concentration deviations $\delta\varphi(\mathbf{x})$ only exist in the presence of a macroscopic concentration gradient and are linear in the macroscopic concentration gradient. As such, we can write

$$\mathbf{J} = -\overline{\rho}\,\mathbf{D}\cdot\nabla c, \tag{40}$$

where the dispersion tensor $\mathbf{D}$ (units of diffusivity) is defined from

$$\mathbf{D}\cdot\nabla c = \frac{-1}{L^3}\int_{\Omega_p}\frac{\rho}{\overline{\rho}}[-D_m\nabla\delta\varphi + \delta\varphi\delta\mathbf{u}]\, d^3\mathbf{x}. \tag{41}$$

This relation is one of the principal results of the paper and will be the starting point for the next section where the individual components D_{ij} are defined in terms of the local fields. The first term in the integral is local diffusion and the second term is what creates mechanical dispersion. To the extent that the local fluid density throughout the pore space is well approximated by the average density $\rho(\mathbf{x}) = \overline{\rho}$, which is the same condition required for neglecting the dispersive flux of solution mass in the total mass balance, the solution density is not involved in the definition of D_{ij}.

If we introduce $\overline{\mathbf{u}} = \mathbf{q}/\phi + \overline{\mathbf{v}}_s$ and allow for a point source of solution injection where c_s is the concentration of solute being injected into a voxel located at $\mathbf{r}_s$ at a volumetric rate Q_s, we then obtain a final macroscopic statement of solute mass balance

$$\frac{\partial c}{\partial t} + \left(\frac{\mathbf{q}}{\phi} + \overline{\mathbf{v}}_s\right)\cdot\nabla c = \frac{1}{\phi\overline{\rho}}\nabla\cdot(\overline{\rho}\mathbf{D}\cdot\nabla c) + \frac{(c_s - c)Q_s}{\phi}\delta(\mathbf{r}-\mathbf{r}_s). \tag{42}$$

V. DEFINITION OF THE DISPERSION TENSOR

The dispersion tensor associated with a given voxel $\Omega(\mathbf{r})$ will be defined here in terms of local fields that have achieved a steady state with respect to the imposed boundary values. If such steady-state has not been achieved, then the operator $\mathbf{D}$ in Eq. (40) would have to be considered a time-convolution operator (or a complex frequency-dependent multiplicative operator in the temporal-frequency domain). As such, we only need to determine the local fields φ and $\mathbf{u}$ when the time derivatives in the local governing equations are zero.

The flow velocity $\mathbf{u}(\mathbf{x})$ satisfies the Navier-Stokes equations throughout the pore space and can be taken, at this local scale, as being incompressible so that

$$\nabla\cdot\mathbf{u} = 0. \tag{43}$$

We further assume that the solution viscosity is independent of φ to leading order so that the flow problem is completely decoupled from the solute concentration problem.

Under the local incompressibility condition, along with the idea that φ does not influence the solution density appreciably, the local fluid density $\rho(\mathbf{x})$ can be modeled as the constant $\overline{\rho}$ so that Eq. (41) becomes

$$\mathbf{D}\cdot\nabla c = \frac{-1}{L^3}\int_{\Omega_p}[-D_m\nabla\delta\varphi + \delta\varphi\,\delta\mathbf{u}]\, d^3\mathbf{x}, \tag{44}$$

where, again, $\delta\varphi = \varphi - c$.

We now divide the porescale concentration field into four contributions

$$\varphi(\mathbf{x}) = c_o + \sum_{i=1}^{3}\delta\varphi_i(\mathbf{x}), \tag{45}$$

where the $\delta\varphi_i$ are solutions of the three Dirichlet subproblems ($i = 1,2,3$):

$$\nabla\cdot(-D_m\nabla\delta\varphi_i + \delta\varphi_i\mathbf{u}) = 0 \quad \text{in}\ \Omega_p \tag{46}$$

$$\delta\varphi_i = \begin{cases}\Delta c_i/2 & \text{on } x_i = \pm L/2\\ 0 & \text{on } x_k = \pm L/2 \quad \text{for } k\neq i\end{cases} \tag{47}$$

and $\mathbf{n}\cdot\nabla\delta\varphi_i = 0$ and $\mathbf{u} = 0$ on ∂G (the grain surfaces). It is easy to verify by direct addition that the sum over the subproblems satisfies Eqs. (33) and (34) in the steady state and when $\nabla\cdot\mathbf{u} = 0$.

For the purpose of analyzing the nature of D_{ij}, we can set $c_o = 0$ with no loss in generality. In this case, we have that $c = \overline{\varphi} = \sum_{i=1}^{3}\overline{\delta\varphi_i}$. Note that in the presence of advection, satisfaction of the Dirichlet boundary conditions on the cube faces can result in $\overline{\delta\varphi_i} \neq 0$. However, when flow is not taking place, we have that $\overline{\delta\varphi_i} = 0$.

To obtain the individual components D_{ij}, we dot multiply Eq. (44) from the left with $\hat{\mathbf{x}}_i$ and use $\nabla c = \Delta c_j\hat{\mathbf{x}}_j/L$ for some particular j. Taking $\Delta c_j \neq 0$ and the concentration drops in the other two directions to be zero defines the $\delta\varphi_j$ subproblem above. As such, we obtain

$$D_{ij} = \frac{-1}{\Delta c_j L^2}\int_{\Omega_p}\hat{\mathbf{x}}_i\cdot[-D_m\nabla\delta\varphi_j + \delta\varphi_j\delta\mathbf{u}]\, d^3\mathbf{x}. \tag{48}$$

The volume integral in Eq. (48) can be written as the average flux across a suite of parallel slices through the material that are

perpendicular to the $\hat{\mathbf{x}}_i$ direction. In the steady state, the flux across each such slice is necessarily the same. For convenience in defining the symmetry properties of D_{ij} in the next section, we rewrite Eq. (48) as the average flux on the two terminal faces of the cube

$$D_{ij} = \frac{-1}{2\Delta c_j L}\left\{ \int_{x_i=+L/2} \hat{\mathbf{x}}_i \cdot [-D_m \nabla \delta\varphi_j + \delta\varphi_j \delta\mathbf{u}]\, d^2\mathbf{x} + \int_{x_i=-L/2} \hat{\mathbf{x}}_i \cdot [-D_m \nabla \delta\varphi_j + \delta\varphi_j \delta\mathbf{u}]\, d^2\mathbf{x} \right\}. \quad (49)$$

This is our final definition of the individual components of the dispersion tensor. In words, component D_{ij} represents the average dispersive flux into and out of the voxel across the terminal faces in the i direction when there is a macroscopic concentration drop in the j direction and no such drops in the other two directions.

From the boundary conditions on the cube faces, the $\delta\varphi_i$ are nonzero only on the two faces $x_i = \pm L/2$. As such, when $i \neq j$, we have that the advection contributions in Eq. (49) are zero so that D_{ij} is only due to diffusion across the cube faces when $i \neq j$. For $i = j$, both diffusion and advection across the cube faces are contributing to the main diagonal components of the dispersion tensor. In this case ($i = j$), because the advective flux will be positive on one face (say, $x_i = +L/2$) and negative on the other (say, $x_i = -L/2$), the diffusive contribution on opposing faces $x_i = \pm L/2$ must be different even in the steady state; i.e., $\hat{\mathbf{x}}_i \cdot \nabla\delta\varphi_j$ will be much bigger on one face compared to the opposing face when $j = i$.

VI. SYMMETRY OF THE DISPERSION TENSOR

To explore the symmetry of the D_{ij}, we focus, say, on the 1,2 pair of subproblems and form the following products:

$$\delta\varphi_2[0 = \nabla \cdot (-D_m \nabla\delta\varphi_1 + \delta\varphi_1 \mathbf{u})], \quad (50)$$

$$\delta\varphi_1[0 = \nabla \cdot (-D_m \nabla\delta\varphi_2 + \delta\varphi_2 \mathbf{u})]. \quad (51)$$

Upon using the identity that $\nabla \cdot (\alpha \mathbf{b}) = \nabla\alpha \cdot \mathbf{b} + \alpha \nabla \cdot \mathbf{b}$, one can show through direct substitution that the following two equations are equivalent to the previous two equations:

$$0 = \nabla \cdot [\delta\varphi_2(-D_m \nabla\delta\varphi_1 + \delta\varphi_1 \mathbf{u})] + D_m \nabla\delta\varphi_2 \cdot \nabla\delta\varphi_1 - \delta\varphi_1 \mathbf{u} \cdot \nabla\delta\varphi_2, \quad (52)$$

$$0 = \nabla \cdot [\delta\varphi_1(-D_m \nabla\delta\varphi_2 + \delta\varphi_2 \mathbf{u})] + D_m \nabla\delta\varphi_1 \cdot \nabla\delta\varphi_2 - \delta\varphi_2 \mathbf{u} \cdot \nabla\delta\varphi_1. \quad (53)$$

Integrating the first term on the right-hand side of these two equations over the cube and applying the divergence theorem, the boundary conditions and Eq. (49), one obtains

$$\int_{\Omega_p} \nabla \cdot [\delta\varphi_2(-D_m \nabla\delta\varphi_1 + \delta\varphi_1 \mathbf{u})] d^3\mathbf{x} = \Delta c_1 \Delta c_2 L D_{21} \quad (54)$$

and

$$\int_{\Omega_p} \nabla \cdot [\delta\varphi_1(-D_m \nabla\delta\varphi_2 + \delta\varphi_2 \mathbf{u})] d^3\mathbf{x} = \Delta c_2 \Delta c_1 L D_{12}. \quad (55)$$

After volume integrating the remaining terms of Eqs. (52) and (53), subtracting and using Eqs. (54) and (55), one has

$$\Delta c_1 \Delta c_2 L(D_{21} - D_{12}) = \int_{\Omega_p} \mathbf{u} \cdot (\delta\varphi_1 \nabla\delta\varphi_2 - \delta\varphi_2 \nabla\delta\varphi_1) d^3\mathbf{x}. \quad (56)$$

The integral on the right-hand side will not be zero, in general, unless $\mathbf{u} = 0$, which is enough to show that D_{21} is generally different from D_{12} at finite Péclet number. Identical manipulations on the other pairs of subproblems leads to

$$\Delta c_i \Delta c_j L(D_{ji} - D_{ij}) = \int_{\Omega_p} \mathbf{u} \cdot (\delta\varphi_i \nabla\delta\varphi_j - \delta\varphi_j \nabla\delta\varphi_i)\, d^3\mathbf{x} \quad (57)$$

for $i \neq j$ so that $D_{ij} \neq D_{ji}$ potentially whenever $\mathbf{u} \neq 0$.

The terms that are entirely responsible for breaking the symmetry of D_{ij} are the advective solute fluxes. Advection breaks the symmetry of the differential operator in the local convection-diffusion equation in the sense above of rendering the operator not to be self-adjoint. The asymmetry of the pore-scale differential operator directly translates into asymmetry of the macroscopic dispersion tensor. When $\mathbf{u} = 0$, only diffusion is at work, the local problem is self-adjoint and $D_{ij} = D_{ji}$ exactly for the off-diagonal terms. There may be off-diagonal components in the purely diffusional case (vanishing Péclet number) if the pore space is anisotropic; e.g., a set of connected fractures having similar orientations that is not aligned with one of the coordinate directions.

The structure of the integrand in Eq. (57) indicates that if there is a systematic variation in the amplitude of $\mathbf{u}$ from one side of the averaging region to the other, or even just a concentration of the flow in one or more places, asymmetry in the D_{ij} can be significantly present at finite Péclet number. As will be performed in a later section, numerical solution of the advection and diffusion at the pore scale is one way to investigate the symmetry of D_{ij} and its relation to the spatial distribution of the flow field $\mathbf{u}$.

Finally, as first suggested in Ref. [14], there is a symmetry that exists in the dispersion tensor. Specifically, if the Reynold's number is sufficiently small that the advective derivative in the Navier-Stokes equation is negligible, then the resulting linear Stokes flow has the property that

$$\mathbf{u}(-\mathbf{f}) = -\mathbf{u}(\mathbf{f}), \quad (58)$$

where $\mathbf{f}$ is the macroscopic force (typically a pressure drop across the voxel) that is driving the porescale flow $\mathbf{u}$. In words, if the sign of the force driving flow is changed, linearity requires the resulting flow velocity to change sign as well. If we go back and change the sign of the flow in the subproblem that defines D_{12} we have

$$\delta\varphi_2[0 = \nabla \cdot (-D_m \nabla\delta\varphi_1 + \delta\varphi_1 \mathbf{u})], \quad (59)$$

$$\delta\varphi_1[0 = \nabla \cdot (-D_m \nabla\delta\varphi_2 - \delta\varphi_2 \mathbf{u})]. \quad (60)$$

Going through the same steps as earlier, one then obtains that

$$\Delta c_1 \Delta c_2 L[D_{21}(\mathbf{f}) - D_{12}(-\mathbf{f})]$$
$$= \int_{\Omega_p} \mathbf{u} \cdot (\delta\varphi_1 \nabla \delta\varphi_2 + \delta\varphi_2 \nabla \delta\varphi_1) d^3\mathbf{x} \quad (61)$$
$$= \int_{\Omega_p} \nabla \cdot (\mathbf{u}\, \delta\varphi_1 \delta\varphi_2) d^3\mathbf{x} \quad (62)$$
$$= \int_{\partial\Omega_p} \mathbf{n} \cdot (\mathbf{u}\, \delta\varphi_1 \delta\varphi_2) d^2\mathbf{x} \quad (63)$$
$$= 0. \quad (64)$$

To get from Eq. (61) to Eq. (62), we require the flow to be incompressible ($\nabla \cdot \mathbf{u} = 0$). To go from Eq. (63) to Eq. (64) we use the boundary condition on the concentration deviations that either $\delta\varphi_1$ or $\delta\varphi_2$ is zero on each of the cube faces.

We have thus demonstrated the flow-reversal symmetry

$$D_{ij}(\mathbf{q}) = D_{ji}(-\mathbf{q}), \quad (65)$$

where the Darcy flux $\mathbf{q}$ is proportional to $\mathbf{f}$ whenever a linear Navier-Stokes equation holds (low Reynolds number). Auriault *et al.* [14] obtain this symmetry to leading order in the Péclet number using an asymptotic two-space homogenization technique. The result of Eq. (65) is independent of Péclet number and applies even when there are multiple length scales of heterogeneity present (where two-space homogenization breaks down). Flekkøy *et al.* [19] also obtain this symmetry using general statistical mechanics arguments attributable to Onsager. Equation (65) places an important constraint on any functional relation for how D_{ij} depends on $\mathbf{q}$.

VII. FUNCTIONAL NATURE OF THE DISPERSION TENSOR

The dispersion tensor is allowing for both the diffusion and advection of solute concentration deviations. To partially separate these two contributions, we write the key $\delta\varphi_i$ concentration deviations as

$$\delta\varphi_i = \frac{\Delta c_i}{L}\left(\Gamma_i + \Gamma_i^{(u)}\right), \quad (66)$$

where Γ_i is independent of the flow and satisfies the boundary-value problem

$$\nabla^2 \Gamma_i = 0 \quad \text{in } \Omega_p \quad (67)$$

$$\Gamma_i = \begin{cases} \pm L/2 & \text{on } x_i = \pm L/2 \\ 0 & \text{on } x_k = \pm L/2 \quad \text{for } k \neq j, \end{cases} \quad (68)$$

while $\Gamma_i^{(u)}$ is the portion influenced by the flow and satisfies

$$\nabla \cdot \left(-D_m \nabla \Gamma_i^{(u)} + \Gamma_i^{(u)} \mathbf{u}\right) = -\nabla \Gamma_i \cdot \mathbf{u} \quad \text{in } \Omega_p \quad (69)$$

$$\Gamma_i^{(u)} = \begin{cases} 0 & \text{on } x_i = \pm L/2 \\ 0 & \text{on } x_k = \pm L/2 \quad \text{for } k \neq j. \end{cases} \quad (70)$$

The sum of Eqs. (67) to (70) when combined with Eq. (66) exactly reproduces Eqs. (46) and (47). The pore-geometry potentials Γ_i are independent of any solute or solution properties in addition to not depending on the flow. The same cannot be said for $\Gamma_i^{(u)}$ that depends on the solute diffusivity D_m in addition to the pore topology and flow field (and, therefore, solution viscosity).

We can now decompose Eq. (49) as $D_{ij} = D_{ij}^{(0)} + D_{ij}^{(u)}$ where

$$D_{ij}^{(0)} = D_m G_{ij} \quad (71)$$

with

$$G_{ij} = \frac{1}{2L^2}\left[\int_{x_i=+L/2} \hat{\mathbf{x}}_i \cdot \nabla \Gamma_j \, d^2\mathbf{x} + \int_{x_i=-L/2} \hat{\mathbf{x}}_i \cdot \nabla \Gamma_j \, d^2\mathbf{x}\right] \quad (72)$$

and where

$$D_{ij}^{(u)} = \frac{-1}{2L^2}\left\{\int_{x_i=+L/2} \hat{\mathbf{x}}_i \cdot \left[-D_m \nabla \Gamma_j^{(u)} + \frac{L}{2}\delta\mathbf{u}\right] d^2\mathbf{x} + \int_{x_i=-L/2} \hat{\mathbf{x}}_i \cdot \left[-D_m \nabla \Gamma_j^{(u)} - \frac{L}{2}\delta\mathbf{u}\right] d^2\mathbf{x}\right\}. \quad (73)$$

We may call G_{ij} the "geometric conductivity tensor." It is the inverse of the "formation factor tensor" F_{ij} and is purely a function of the pore topology. It may be written more compactly as

$$G_{ij} = F_{ij}^{-1} = \frac{1}{L^3}\int_{\Omega_p} \nabla \Gamma_i \cdot \nabla \Gamma_j \, d^3\mathbf{x}. \quad (74)$$

To get from Eq. (74) to Eq. (72), we write $\nabla\Gamma_i \cdot \nabla\Gamma_j = \nabla \cdot [\Gamma_i \nabla \Gamma_j] - \Gamma_i \nabla^2 \Gamma_j$, note that $\nabla^2\Gamma_j = 0$, use the divergence theorem and apply the boundary conditions for Γ_i. Without even using the symmetry argument from the previous section (that nonetheless applies), we obtain the symmetry $G_{ij} = G_{ji}$ due to the fact that $\mathbf{a} \cdot \mathbf{b} = \mathbf{b} \cdot \mathbf{a}$.

For an isotropic material, we have

$$G = \frac{1}{F} = \frac{1}{L^3}\int_{\Omega_p} \nabla \Gamma_i \cdot \nabla \Gamma_i \, d^3\mathbf{x} \quad (75)$$

for any of $i = 1$, 2, or 3 and where F is the formation factor. The formation factor is often modeled using Archie's Law [20] as $F = \phi^{-m}$ where $3/2 \leqslant m \leqslant 2$ for most granular media. The formation factor is sometimes expressed $F = \tau/\phi$ where τ is called the tortuosity.

Although $D_{ij}^{(0)}$ factors into a solute property D_m and a pore-geometry term G_{ij}, the same does not hold true for $D_{ij}^{(u)}$. For a flow field where

$$\int_{x_i=+L/2} \hat{\mathbf{x}}_i \cdot \delta\mathbf{u} \, d^2\mathbf{x} = \int_{x_i=-L/2} \hat{\mathbf{x}}_i \cdot \delta\mathbf{u} \, d^2\mathbf{x}, \quad (76)$$

we can rewrite Eq. (73) as

$$D_{ij}^{(u)} = D_m G_{ij}^{(u)}, \quad (77)$$

where

$$G_{ij}^{(u)} = \frac{1}{2L^2}\left[\int_{x_i=+L/2} \hat{\mathbf{x}}_i \cdot \nabla \Gamma_j^{(u)} \, d^2\mathbf{x} + \int_{x_i=-L/2} \hat{\mathbf{x}}_i \cdot \nabla \Gamma_j^{(u)} \, d^2\mathbf{x}\right]. \quad (78)$$

Because the potential field $\Gamma_j^{(u)}$ has all of D_m, flow and pore-topology dependence entangled within it as Eq. (69) makes clear, so does $G_{ij}^{(u)}$. Further, we cannot rewrite $G_{ij}^{(u)}$ in the compact form of Eq. (74) because $\nabla^2 \Gamma_j^{(u)} = -(\Gamma_j + \Gamma_j^{(u)}) \cdot \mathbf{u}/D_m \neq 0$.

In an isotropic porous material, the dispersion tensor is usually assumed to take (but not proven to have) the symmetric "standard form" [1,10,11]

$$\mathbf{D} \approx \mathbf{D}^{st} \equiv \frac{D_m}{F}\mathbf{I} + \gamma_l \frac{|\mathbf{q}|}{\phi}\hat{\mathbf{x}}_q\hat{\mathbf{x}}_q + \gamma_t \frac{|\mathbf{q}|}{\phi}(\mathbf{I} - \hat{\mathbf{x}}_q\hat{\mathbf{x}}_q), \quad (79)$$

where

$$\hat{\mathbf{x}}_q = \frac{\mathbf{q}}{|\mathbf{q}|} \quad (80)$$

is a unit vector in the direction of the Darcy flow, $\mathbf{I}$ is the identity tensor, and γ_l and γ_t are the so-called longitudinal and transverse "dispersivities" that have units of length. The first term involving F is without reproach but the second and third terms involving the dispersivities are conjectural. Delgado [21] has compiled laboratory dispersion data from the literature for sands and bead packs and finds that

$$\gamma_l \approx 2\ell, \quad (81)$$

$$\gamma_t \approx \frac{\ell}{40} \quad (82)$$

fits the data fairly well over the range of roughly $50 < \mathrm{Pe} < 10^5$ when ℓ is taken as a characteristic grain diameter. At such large Pe, the advection is dominating the diffusion and is why the dispersivities are independent of D_m (or Pe). At intermediate values of Pe, where advection and diffusion are more comparable, the simple model of Eqs. (81) and (82) breaks down and the dispersivities have a more complicated Pe dependence that has not been theoretically determined for arbitrary porous materials. Further, as the scale of a plume increases, the length parameter ℓ in the dispersivities is experimentally observed to increase in size [22].

The above standard form for the dispersion tensor satisfies both $D^{st}_{ij}(\mathbf{q}) = D^{st}_{ji}(\mathbf{q})$ and $D^{st}_{ij}(\mathbf{q}) = D^{st}_{ji}(-\mathbf{q})$. If one of the coordinate directions is made to align with the flow direction $\hat{\mathbf{x}}_q$, Eq. (79) produces a purely diagonal dispersion tensor that is anisotropic (the various components D^{st}_{11}, D^{st}_{22}, and D^{st}_{33} may all be different). The symmetries are trivially satisfied because there are no off-diagonal components in this case. Implicitly, the form of Eq. (79) is only allowing for the dispersive flux that is in the same direction as the concentration gradient present and is ignoring any possible cross flux across the faces that are perpendicular to the concentration gradient.

However, if flow in a given direction is stronger on one side of a voxel than it is on the other side, then even if one of the coordinates is in the $\hat{\mathbf{x}}_q$ direction, there will be off-diagonal components of the dispersion tensor (flux in a direction different than the concentration gradient) and Eqs. (57) and (65) inform us to expect these off-diagonal components to satisfy the symmetry constraints that $D_{ij}(\mathbf{q}) \neq D_{ji}(\mathbf{q})$ and $D_{ij}(\mathbf{q}) = D_{ji}(-\mathbf{q})$.

We thus expect that in addition to the dependence on the mean flow $\mathbf{q}$ as expressed in the standard form $\mathbf{D}^{st}$, there is also a dependence on the macroscopic flow gradient that leads to of-diagonal terms of $\mathbf{D}$ even in isotropic media and that we conjecture has the form

$$\mathbf{D} \approx \mathbf{D}^{st} - \alpha[\nabla\mathbf{q} - (\nabla\mathbf{q})^T], \quad (83)$$

where α is a positive parameter that has the units of length squared. Equation (83) is suggesting that when one of the spatial coordinates is aligned with the average flow direction so that Eq. (79) has no off-diagonal terms in an isotropic material, the off-diagonal terms are due entirely to the presence of a flow gradient across the system and that D_{ij} is anti-symmetric (equal in amplitude and opposite in sign) to D_{ji}. We will test this hypothesis numerically in the examples that follow.

We will also test to see whether the length $\sqrt{\alpha}$ itself depends on the flow gradient. We expect that as the flow gradient increases, high (or low) solute concentration becomes increasingly pushed up against the $\delta\varphi = 0$ Dirichlet conditions on the lateral sides of the cube. As the flow-induced concentration gradients at the lateral walls become larger with increasing flow gradient, we expect the off-diagonal components of the dispersion tensor to increase. Whether such increases are linear in the applied flow gradient will be numerically investigated.

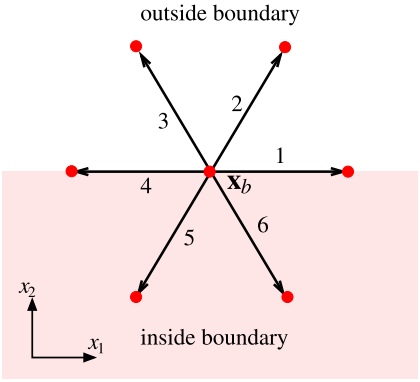

FIG. 2. The D2Q6 triangular lattice focusing on a particular node $\mathbf{x}_b$ sitting on the boundary surrounded by the six links $i = 1,6$ that have total mass populations N_i and solute mass concentrations Δ_i. The constant velocities $\mathbf{c}_i$ are shown as arrows and are given by $\mathbf{c}_1 = \hat{\mathbf{x}}_1, \mathbf{c}_2 = \hat{\mathbf{x}}_1/2 + \sqrt{3}\hat{\mathbf{x}}_2/2, \mathbf{c}_3 = -\hat{\mathbf{x}}_1/2 + \sqrt{3}\hat{\mathbf{x}}_2/2, \mathbf{c}_4 = -\hat{\mathbf{x}}_1, \mathbf{c}_5 = -\hat{\mathbf{x}}_1/2 - \sqrt{3}\hat{\mathbf{x}}_2/2, \mathbf{c}_6 = \hat{\mathbf{x}}_1/2 - \sqrt{3}\hat{\mathbf{x}}_2/2$.

VIII. LATTICE-BOLTZMANN NUMERICAL EXAMPLES

We now numerically solve the suite of three independent subproblems given by Eqs. (46)–(47). The flow velocity is driven by an applied force $\mathbf{f}$. We use lattice-Boltzmann simulations to solve for the local concentration deviations, fluid flow throughout the pore space and the components D_{ij} of the dispersion tensor using Eq. (49) or Eq. (48). For the purpose of analyzing the symmetry of D_{ij}, two-dimensional simulations are sufficient.

A. Lattice-Boltzmann flux calculations

The lattice-Boltzmann model for miscible binary fluids is well known and described in many places [23–25]. Here we mainly focus on how the boundary conditions are implemented.

Employing a triangular D2Q6 lattice with unit vectors $\mathbf{c}_i$, $i = 1,\ldots,6$ connecting the nodes of the lattice (cf. Fig. 2), two populations are defined, N_i and Δ_i with $i = 1,\ldots,6$. The first of these govern the mass and momentum densities according

to the following definitions

$$\rho(\mathbf{x},t) = \sum_{i=1}^{6} N_i(\mathbf{x},t) \tag{84}$$

and

$$\rho(\mathbf{x},t)\mathbf{u}(\mathbf{x},t) = \sum_{i=1}^{6} N_i(\mathbf{x},t)\mathbf{c}_i. \tag{85}$$

The second population gives rise to a concentration

$$\varphi(\mathbf{x},t) = \sum_{i=1}^{6} \Delta_i(\mathbf{x},t), \tag{86}$$

defined here as the ratio of solute mass to total mass present at each site. We will not pause here to give the lattice-Boltzmann update equations for the N_i and Δ_i populations.

The solute flux through a given site is the average of the in- and outgoing solute populations defined in the following way:

$$\mathbf{j}(\mathbf{x},t) \equiv -D_m \nabla\varphi(\mathbf{x},t) + \varphi(\mathbf{x},t)\mathbf{u}(\mathbf{x},t) \tag{87}$$

$$= \frac{1}{2}\sum_{i=1}^{6} \mathbf{c}_i[\Delta_i(\mathbf{x},t) + \Delta_i'(\mathbf{x},t)]. \tag{88}$$

Here $\Delta_i(\mathbf{x},t)$ is the precollision population and $\Delta_i'(\mathbf{x},t)$ the postcollision population defined as

$$\Delta_i'(\mathbf{x},t) = \Delta_i(\mathbf{x},t) + \lambda_D\big[\Delta_i(\mathbf{x},t) - \Delta_i^{eq}(\varphi,\mathbf{u})\big], \tag{89}$$

where $\Delta_i^{eq}(\varphi,\mathbf{u})$ is the equilibrium population which in the Flekkøy (1993) scheme is given by

$$\Delta_i^{eq} = w_i\,\varphi(\mathbf{x},t)\left[1 + \frac{\mathbf{u}(\mathbf{x},t)\cdot\mathbf{c}_i}{c_s^2}\right]. \tag{90}$$

Here, w_i are the lattice weights given by $w_i = 1/6$ for the triangular lattice and $c_s = \Delta x/(\Delta t\sqrt{2})$ is the speed of sound on the triangular lattice with $\Delta x = 1$ and $\Delta t = 1$ the lattice spacing and time step in lattice units. The relaxation parameter λ_D controls the particle collisions and determines the molecular diffusivity in the scheme. Inserting Eq. (89) into Eq. (88) gives

$$\mathbf{j} = \frac{(2+\lambda_D)}{2}\sum_{i=1}^{6} \mathbf{c}_i\big(\Delta_i - \Delta_i^{eq}\big) + \sum_{i=1}^{6} \mathbf{c}_i\Delta_i^{eq} \tag{91}$$

$$= \frac{(2+\lambda_D)}{2}\sum_{i=1}^{6} \mathbf{c}_i\Delta_i^{\mathrm{neq}} + \varphi\mathbf{u}. \tag{92}$$

The second summation in Eq. (91) was performed exactly using Eq. (90) and thus corresponds to solute advection. The first summation that depends only on the nonequilibrium portion of the populations corresponds to solute diffusion. A Chapman-Enskog expansion of the lattice-Boltzmann update equations for the Δ_i gives the conservation law

$$\partial_t\varphi + \nabla\cdot\mathbf{j} = 0, \tag{93}$$

along with an expression for the molecular diffusivity

$$D_m = -\frac{(2+\lambda_D)}{2\lambda_D}c_s^2\Delta t. \tag{94}$$

On an $M_1 \times M_2$ lattice, the dispersion tensor components are calculated using

$$D_{ij} = \frac{L_j}{\Delta c_j}\frac{1}{2M_j}\sum_{b=1}^{2M_j} \hat{\mathbf{x}}_i\cdot\mathbf{j}(\mathbf{x}_b,t), \tag{95}$$

where $\mathbf{x}_b$ are the site positions on the two bounding faces located at $x_i = \pm L_i/2$. For the triangular lattice, the side lengths are $L_1 = M_1$ and $L_2 = (\sqrt{3}/2)M_2$ (cf. Fig. 2). The concentration drops Δc_j are as given in Eq. (34).

On the system boundaries, φ satisfies Dirichlet conditions of the form $\varphi(\mathbf{x}_b) = C_b$ with C_b some desired boundary value. To satisfy such a condition one should not just set the boundary populations as $\Delta_i(\mathbf{x}_b) = w_i C_b$ because although this will indeed satisfy the boundary condition for φ, it does not allow for diffusion across the boundary.

To calculate the normal component of flux $\mathbf{n}\cdot\mathbf{j}$ at boundary points where $\varphi(\mathbf{x}_b) = C_b$, we first note that at any boundary point, the lattice-Boltzmann equation produces updates for the Δ_i populations on half of the links, say, $i = 1,2,3$, using population data from sites interior to the system domain. To properly handle diffusion across such boundaries, we then prescribe values for the other three links from the requirement that

$$\mathbf{n}\cdot\sum_{i=1}^{3} \mathbf{c}_i\Delta_i^{\mathrm{neq}}(\mathbf{x}_b) = \mathbf{n}\cdot\sum_{i=1}^{3} \mathbf{c}_{i+3}\Delta_{i+3}^{\mathrm{neq}}(\mathbf{x}_b). \tag{96}$$

In words, the diffusive contribution from populations on links that are being updated is identical to the contribution from the populations that are not being updated. This is equivalent to saying that the flux is locally uniform across the boundary. Because $\mathbf{c}_{i+3} = -\mathbf{c}_i$, we then obtain that

$$\Delta_{i+3}(\mathbf{x}_b) = \Delta_{i+3}^{eq}(\mathbf{x}_b) + \Delta_i^{eq}(\mathbf{x}_b) - \Delta_i(\mathbf{x}_b), \tag{97}$$

where

$$\Delta_{i+3}^{eq}(\mathbf{x}_b) = w_i C_b\left[1 - \frac{\mathbf{u}(\mathbf{x}_b)\cdot\mathbf{c}_i}{c_s^2}\right], \tag{98}$$

$$\Delta_i^{eq}(\mathbf{x}_b) = w_i C_b\left[1 + \frac{\mathbf{u}(\mathbf{x}_b)\cdot\mathbf{c}_i}{c_s^2}\right] \tag{99}$$

so that the proper boundary condition that allows for diffusive flux across the Dirichlet boundary is

$$\Delta_{i+3} = 2w_i C_b - \Delta_i. \tag{100}$$

Equation (92) can then be written

$$\mathbf{j}(\mathbf{x_b}) = (2+\lambda_D)\sum_{i=1}^{3} \mathbf{c}_i\Delta_i^{\mathrm{neq}}(\mathbf{x}_b) + C_b\mathbf{u}(\mathbf{x}_b), \tag{101}$$

and this expression for $\mathbf{j}$ is then used to calculate the dispersion-tensor components of Eq. (95). For each face of the $L_1 \times L_2$ box, the boundary conditions are given in Table I.

A final problem remains that limits the accuracy of the D_{ij} calculations at large Pe. At large Pe, a given solute concentration is pushed up against the $\varphi = 0$ or $\pm\,\Delta c_i$ boundaries which results in large concentration gradients near some of the boundaries. At large enough Pe, the distance over which φ changes becomes comparable to (or smaller than) the lattice spacing. In the lattice-Boltzmann model being employed [23],

TABLE I. Boundary populations for the D2Q6 lattice that satisfy the Dirichlet condition $\varphi(\mathbf{x}_b) = C_b$.

Face	LBE determined populations	BC determined populations
$x_2 = +L_2/2$	$\Delta_2, \Delta_3, \Delta_1$	$\Delta_5 = C_b/3 - \Delta_2$ $\Delta_6 = C_b/3 - \Delta_3$ $\Delta_4 = C_b/3 - \Delta_1$
$x_2 = -L_2/2$	$\Delta_5, \Delta_6, \Delta_4$	$\Delta_2 = C_b/3 - \Delta_5$ $\Delta_3 = C_b/3 - \Delta_6$ $\Delta_1 = C_b/3 - \Delta_4$
$x_1 = +L_1/2$	$\Delta_1, \Delta_2, \Delta_6$	$\Delta_4 = C_b/3 - \Delta_1$ $\Delta_5 = C_b/3 - \Delta_2$ $\Delta_3 = C_b/3 - \Delta_6$
$x_1 = -L_1/2$	$\Delta_4, \Delta_5, \Delta_3$	$\Delta_1 = C_b/3 - \Delta_4$ $\Delta_2 = C_b/3 - \Delta_5$ $\Delta_6 = C_b/3 - \Delta_3$

this causes unwanted higher-order derivatives to enter into the advection-diffusion equation as made evident through the Chapman-Enskog expansion of the algorithm. The only cure for this is to increase the resolution of the lattice by increasing the number of nodes contained within the $L_1 \times L_2$ box. This remains the main source of error in the flux calculations that follow and gets worse with increasing Pe.

In the simulations, we work with

$$\nu = \frac{\eta}{\rho} = 0.1\ \Delta x^2/\Delta t, \tag{102}$$

$$D_m = 0.02\Delta x^2/\Delta t, \tag{103}$$

where ν is the kinematic viscosity (or viscous diffusivity), $\Delta x = 1$ is the lattice constant and $\Delta t = 1$ the time step. The key dimensionless numbers that control the nature of the dispersive flux are the Péclet number and the Reynolds number given by

$$\mathrm{Pe} \equiv \frac{|\varphi \mathbf{u}|}{|D_m \boldsymbol{\nabla}\varphi|} \approx \frac{U_{\max} L}{D_m}, \tag{104}$$

$$\mathrm{Re} \equiv \frac{|\rho \mathbf{u}\cdot\boldsymbol{\nabla}\mathbf{u}|}{|\eta\nabla^2\mathbf{u}|} \approx \frac{U_{\max} L}{\nu} = \frac{D_m}{\nu}\mathrm{Pe} = \frac{\mathrm{Pe}}{5}, \tag{105}$$

where $U_{\max}$ is the maximum flow speed in the simulation domain and L is a typical grain size except in those simulations where there are no solid grains in which case we take it to be the system size. When there are solid obstacles present, we want Re to be less than one so that we are in the laminar flow regime where flow reversal occurs when the force driving the flow is reversed. This then limits the maximum Pe we can consider to say Pe = 3 according to Eq. (105). When there are no solid obstacles present, the flow considered in the simulations is independent of Re (the rate of momentum advection $\rho\mathbf{u}\cdot\boldsymbol{\nabla}\mathbf{u}$ is identically zero) and we can increase Pe to much larger values by increasing the flow velocity (force driving the flow). However, as discussed above, at larger Pe, the concentration gradient near the boundaries becomes large and its numerical simulation is limited by the lattice spacing. In the numerical simulations given below, this effect limits us to the regime of, say, Pe < 40.

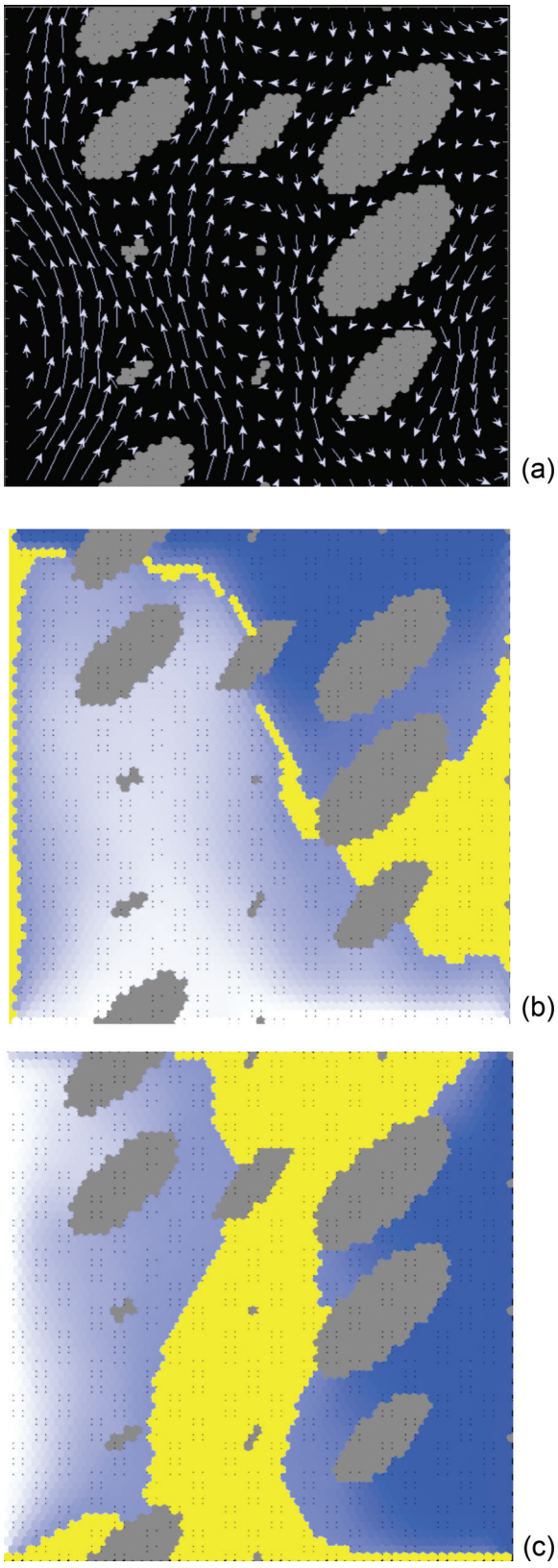

FIG. 3. Sinusoidal forcing $\mathbf{f} = \hat{\mathbf{x}}_2 \sin(2\pi x_1/L)$ with Pe = 3.0. (a) The flow field. (b) The concentration distribution near steady state when the applied concentration gradient is in the vertical direction. (c) When the concentration gradient is in the horizontal direction. Yellow denotes zero concentration, white positive, and blue negative concentration.

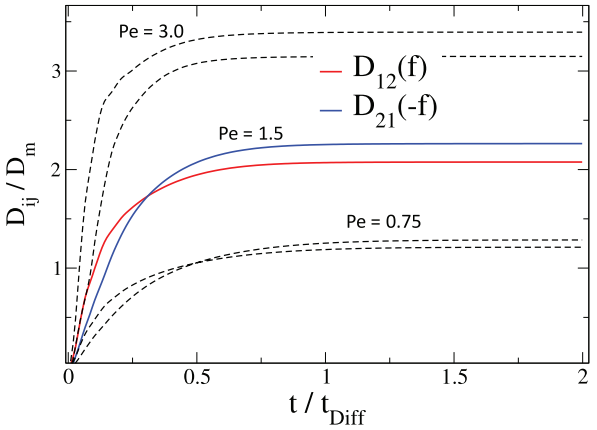

FIG. 4. The dispersion components corresponding to the geometry and forcing in Fig. 3 but with $\mathrm{Pe} = q_{\max} L_1/D_m = 0.75$, 1.5, and 3.0 from bottom to top. The diffusion time constant is defined $t_{\mathrm{Diff}} = L_1^2/D_m$. The lower curve near the origin is $D_{21}(-f)$ for each Pe.

B. Simulations of the off-diagonal components D_{ij}

Larger flow velocity gradients within the system produce larger values of the off-diagonal components D_{ij}. In Fig. 3 we employ a sinusoidal forcing field to produce such flow gradients in a nontrivial pore-space geometry. The flow field and the concentration distribution in steady state are shown with concentration drops in both the vertical and horizontal directions. In Fig. 4 the flow-reversal symmetry $D_{ij}(f) = D_{ji}(-f)$ is demonstrated with discrepancy increasing with increasing Pe as the concentration gradients get larger near the edges of the system. Going to smaller lattice spacing at higher values of Pe is observed to reduce the discrepancy.

To explore the conjecture of Eq. (83), that the nondiagonal part of the dispersion tensor has the form $\alpha[\nabla \mathbf{q} - (\nabla \mathbf{q})^T]$, we introduce a linear gradient in the flow velocity and remove all solid obstacles since satisfying the boundary conditions on the grain surfaces is another source of numerical error. In this scenario, because there are no solid grains present, we use the system size as the length in the definition of Pe. If we equate $\mathbf{q}$ and $\mathbf{u}$ under these conditions, we assume a flow field of the form

$$q_2(x_1) = q_o + \frac{\Delta q_2}{L_1} x_1. \tag{106}$$

The flow field and concentration distribution in this scenario for concentration gradients in the vertical and horizontal directions are shown in Fig. 5. The off-diagonal dispersion-tensor components are then plotted in Fig. 6 both for normal forcing $+f$ and reversed forcing $-f$. Figure 6 demonstrates that the off-diagonal components are indeed antisymmetric and satisfy the flow-reversal symmetry as Eq. (83) predicts. The results when the force driving the flow is reversed have an error associated with them (the observed wiggles) that increases with increasing Pe. This error is a lattice-Boltzmann artifact.

We have verified numerically that if there is no flow gradient ($\Delta q_2 = 0$) and only a uniform flow q_o present, the off-diagonal components are zero as is also expected analytically. We have also verified that in the presence of a flow gradient ($\Delta q_2 \neq 0$), the off-diagonal components are independent of q_o and are monotonic in Δq_2. Indeed, when we plot the steady-state off-diagonal terms D_{12} and D_{21} in Fig. 7 as a function of

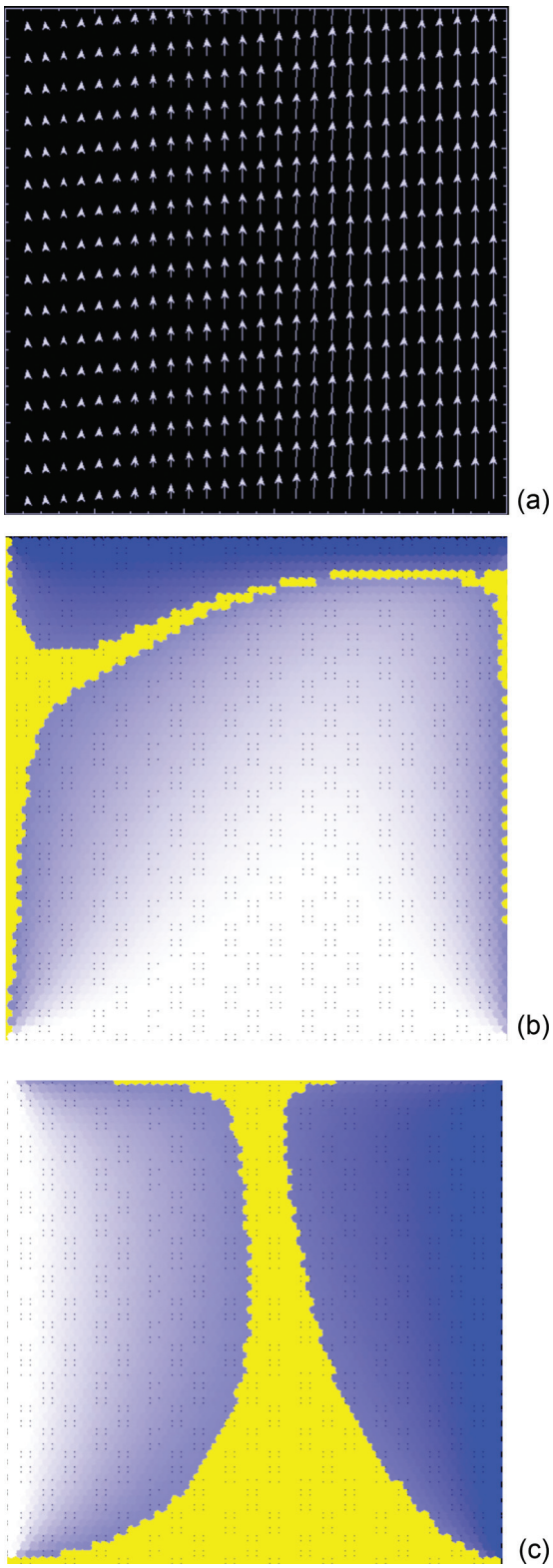

FIG. 5. (a) The flow field corresponding to Eq. (106) when no solid obstacles are present. (b) The concentration field near steady state when there is an imposed concentration gradient in the vertical direction (in the same direction as the flow field). (c) When the concentration gradient is in the horizontal direction.

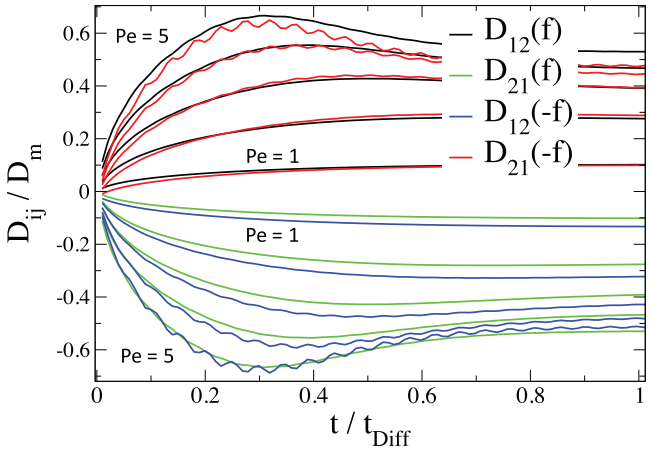

FIG. 6. The dispersion coefficients corresponding to the geometry and forcing in Fig. 5 with $\mathrm{Pe} = \Delta q_2 L_1/D_m$ ranging from 1 to 5. The wiggles in the reversed-flow $(-f)$ results is a numerical artifact.

$\mathrm{Pe} = |\nabla \mathbf{q}| L_1^2/D_m = |\Delta q_2| L_1/D_m$, we observe that D_{21} exhibits the functional dependence on Pe given by

$$\frac{D_{21}(\mathrm{Pe})}{D_m} = \mathrm{Pe}(0.15 - 0.034 \ln \mathrm{Pe}) \tag{107}$$

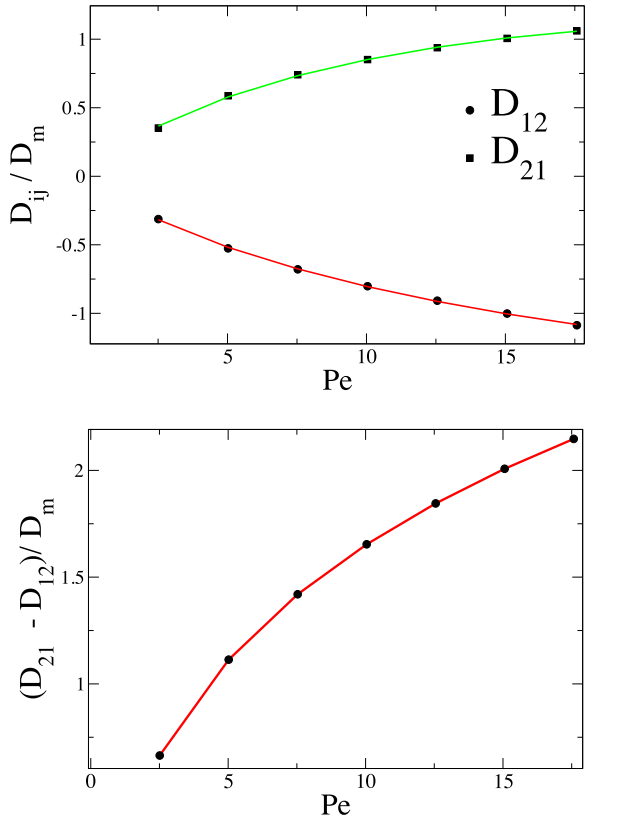

FIG. 7. Upper panel: The off-diagonal components $D_{12}(f)$ and $D_{21}(f)$ as a function of Pe. The data fits are made using $D_{21} = \mathrm{Pe}(a + b \ln \mathrm{Pe})$ with a and b given by Eq. (107). The numerical results demonstrate the anti-symmetric behavior $D_{12}(f) \approx -D_{21}(f)$. Lower panel: The difference $[D_{21}(f) - D_{12}(f)]/D_m$ [which is $\approx 2D_{21}(f)/D_m$]. Both panels correspond to the steady-state behavior observed in Fig. 6.

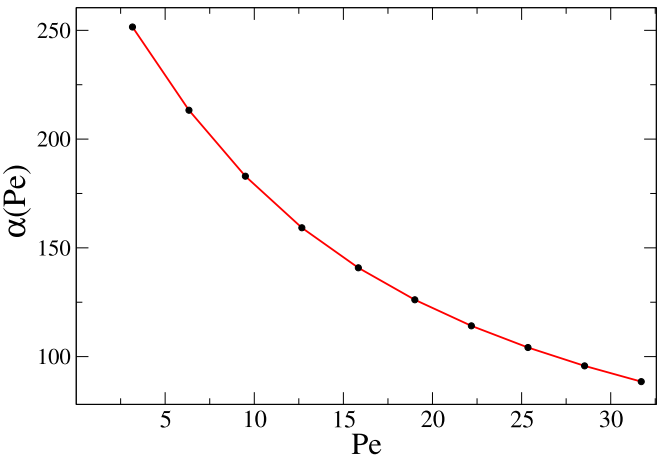

FIG. 8. The $\alpha(\mathrm{Pe})$ coefficient corresponding to Fig. 6 and obtained from Eq. (111).

with a similar fit to D_{12} other than for the antisymmetric behavior that $D_{12} \approx -D_{21}$.

For the above modeling scenario, the conjecture of Eq. (83) takes the form

$$D_{12} = -\alpha \frac{\Delta q_2}{L_1}, \tag{108}$$

$$D_{21} = \alpha \frac{\Delta q_2}{L_1}, \tag{109}$$

where the sign of the force driving flow is the same for both D_{12} and D_{21}. We then have

$$\frac{D_{21} - D_{12}}{D_m} = 2\alpha \frac{\Delta q_2}{D_m L_1}, \tag{110}$$

so that upon using the definition that $\mathrm{Pe} = \Delta q_2 L_1/D_m$ we have

$$\alpha(\mathrm{Pe}) = \frac{L_1^2}{2\mathrm{Pe}} \frac{(D_{21} - D_{12})}{D_m}. \tag{111}$$

The result is shown in Fig. 8. The function $\alpha(\mathrm{Pe})$ is monotonically decreasing in Pe and this is due to the Pe dependence of $D_{21} - D_{12}$ not being purely linear in the flow gradient but also having a logarithmic dependence. The numerical data is well fit by the function

$$\alpha(\mathrm{Pe}) = \Delta x^2 (330 - 74 \ln \mathrm{Pe}), \tag{112}$$

where $\Delta x = 1$ in lattice units. The range of $2 < \mathrm{Pe} < 35$ explored in Fig. 8 represents the maximum Pe we can treat at a given resolution of the lattice-Boltzmann simulations due to the diffusion lengths near the $\varphi = 0$ lateral boundaries (i.e., the distance over which the concentration gradients have significant support) becoming smaller than the lattice spacing at higher ranges of Pe. How the diffusive flux across lateral boundaries increases as the lateral-boundary concentration gradients increase with increasing Pe is not explicitly allowed for in the model of Eq. (83) and as such more work is required to understand the observed logarithmic $\alpha(\mathrm{Pe})$ dependence.

IX. CONCLUSIONS

The numerical simulations show that when one of the coordinate axes aligns with the mean direction of flow, to

obtain nonzero off-diagonal components of the dispersion tensor in an isotropic system requires a gradient in flow to be present across the system. We showed analytically that the off-diagonal components satisfy the flow-reversal symmetry $D_{ij}(+q) = D_{ji}(-q)$ at any Péclet number. We then conjectured that the off-diagonal components have the analytical form $\alpha[\nabla\mathbf{q} - (\nabla\mathbf{q})^T]$ which is both antisymmetric and satisfies the flow-reversal symmetry. The numerical results confirmed this conjecture but showed α to be not just a constant but to have an additional logarithmic dependence on the flow-gradient amplitude over the range $2 < \mathrm{Pe} < 35$ that was treated numerically. Analytical predictions of such logarithmic nonlinearity in the flow-gradient dependence of the dispersion tensor components were not provided in this study. In ongoing work, we will further pursue how the dispersion tensor depends on the nature of the flow field in higher-accuracy finite-volume numerical simulations of the pore-scale transport.

In addition to these discoveries about the dispersion tensor, we also obtain the solute mass conservation laws at the macroscopic scale under conditions when the pore-space geometry and fluid density are possibly changing. However, to address the symmetry properties of the dispersion tensor, we assume any sources of nonlinearity in the system, such as evolving pore topology or changing fluid density, are absent because nonlinear response renders the transport tensor asymmetric. Although the fluid flow is assumed to be decoupled from the evolving solute concentrations in the analysis of the dispersion tensor symmetry, the presence of advection by itself is enough to cause the dispersion tensor to be asymmetric. This is because the advection makes the pore-scale differential operator controlling the changes in solute concentration to be asymmetric.

ACKNOWLEDGMENTS

The work of S.R.P. and D.W.V. was supported entirely by the U.S. Department of Energy, Office of Science, Office of Basic Energy Sciences, Chemical Sciences, Geosciences and Biosciences Division under Contract DE-AC02-05CH11231.

[1] J. Bear, *Dynamics of Fluids in Porous Media* (American Elsevier, New York, 1965).
[2] G. de Marsily, *Quantitative Hydrogeology* (Academic Press, San Diego, 1986).
[3] F. A. L. Dullien, *Porous Media: Fluid Transport and Pore Structure* 2nd ed. (Academic Press, San Diego, 1992).
[4] M. Sahimi, *Flow and Transport in Porous Media and Fractured Rock* (Wiley-VCH, New York, 2011).
[5] G. A. Truskey, F. Yuan, and D. F. Katz, *Transport Phenomena in Biological Systems* (Pearson Prentice Hall, Upper Saddle River, NJ, 2004).
[6] C. Tien, *Principles of Filtration* (Elsevier, Amsterdam, 2012).
[7] R. Aris, Proc. Roy. Soc. A **235**, 67 (1956).
[8] B. Bijeljic, P. Mostaghimi, and M. J. Blunt, Phys. Rev. Lett. **107**, 204502 (2011).
[9] D. W. Meyer and B. Bijeljic, Phys. Rev. E **94**, 013107 (2016).
[10] A. E. Scheidegger, J. Geophys. Res. **66**, 3273 (1961).
[11] J. Bear, J. Geophys. Res. **66**, 1185 (1961).
[12] S. Whitaker, AIChE Journal **13**, 420 (1967).
[13] C. C. Mei, Transp. Transp. Porous Media **9**, 261 (1992).
[14] J.-L. Auriault, C. Moyne, and H. A. Souto, Transp. Porous Med. **85**, 771 (2010).
[15] S. R. Pride and J. G. Berryman, J. Mech. Phys. Solids **46**, 719 (1998).
[16] S. R. Pride, J. G. Berryman, M. Commer, S. Nakagawa, G. A. Newman, and D. W. Vasco, Geophys. Prospect. (2016), doi:10.1111/1365-2478.12435.
[17] M. A. Biot and D. G. Willis, J. Appl. Mech. **24**, 594 (1957).
[18] L. D. Landau and E. M. Lifshitz, *Fluid Mechanics*, 2nd ed. (Pergamon, New York, 1987).
[19] E. G. Flekkøy, S. R. Pride, and R. Toussaint, Phys. Rev. E **95**, 022136 (2017).
[20] G. E. Archie, Trans. AIME **146**, 54 (1942).
[21] J. M. P. Q. Delgado, Chem. Eng. Res. Design **85**, 1245 (2007).
[22] L. W. Gelhar, C. Welty, and K. R. Rehfeldt, Water Resour. Res. **28**, 1955 (1992).
[23] E. G. Flekkøy, Phys. Rev. E **47**, 4247 (1993).
[24] D. H. Rothman and S. Zaleski, *Lattice-Gas Cellular Automata: Simple Models of Complex Hydrodynamics*, Vol. 5 (Cambridge University Press, Cambridge, 1997).
[25] B. Chopard, J. Falcone, and J. Latt, Eur. Phys. J. Special Topics **171**, 245 (2009).